

IN SEARCH OF THE DARK AGES – AN EXPERIMENTAL CHALLENGE

J. BLAND-HAWTHORN

Anglo-Australian Observatory, P.O. Box 296, Epping, NSW 2121, Australia

AND

P.E.J. NULSEN¹

Harvard-Smithsonian Center for Astrophysics, 60 Garden Street, Cambridge, MA 02138

Draft version November 13, 2018

ABSTRACT

Most direct source detections beyond $z \sim 7$ are likely to arise from wide-field narrowband surveys of Ly α emission in the J band. For this to be true, the Ly α emission must somehow escape from compact star-forming regions (CSR) presumably associated with massive haloes. Since the Ly α escape fraction is $\lesssim 10\%$ from an emitting region of size ~ 1 kpc, these objects will be difficult to find and hard to detect, requiring $\sim 30 - 100$ hours at each telescope pointing on $8 - 10$ m telescopes. For CSR sources, existing large-format IR arrays are close to ideal in terms of their noise characteristics for conducting *wide-field* narrowband surveys where pixel sizes are $0.1''$ or larger.

However, we stress that Ly α can also arise from external large-scale shocks (ELS) due to starburst winds, powered by CSRs, ploughing into gas actively accreting onto the dark halo. The winds effectively carry energy from the dense, dusty environment of a starburst into lower density regions, where the escape probability for Ly α photons is greater. ELS emission is expected to be considerably more clumpy ($\lesssim 100$ pc) than CSR emission. For ELS sources, IR arrays will need $1 - 2$ orders of magnitude improvement in dark current in order to detect dispersed clumpy emission within the environments of massive haloes. These sources require an IR camera with small pixels ($\sim 0.01''$) and adaptive optics correction (*e.g.*, GSAOI on Gemini), and will therefore require a *targetted* observation of a Dark Age source identified by a wide-field survey. For either targetted or wide-field surveys, the deepest observations will be those where the pixel sampling is well matched to the size of the emitting regions. We show that there are only $3 - 4$ J-band windows [$z = 7.72, (8.22), 8.79, 9.37$] suitable for observing the Dark Ages in Ly α ; we summarize their cosmological properties in Table 1.

Subject headings: cosmology; first stars; intergalactic medium; galaxies — high redshift

1. INTRODUCTION

In recent years, we have come to recognize that the ‘ionization epoch’ may lie just beyond our current observational horizon (*cf.* Fan *et al.* 2000, 2003; Kneib *et al.* 2004). Structure formation models in CDM cosmologies appear to show that this epoch took place at $z = 7 - 12$ (Gnedin & Ostriker 1997; Haiman & Loeb 1998). Recent wide-angle polarization measurements with WMAP (Kogut *et al.* 2003) suggest the ionization epoch could have been well under way by $z \sim 17$. However, this may conflict with the inferred high column densities in $z \sim 6$ quasars (*e.g.*, Wyithe & Loeb 2004). Since cosmic ionization requires only a tiny fraction of the primordial gas to be converted into stars or black holes (Loeb & Barkana 2001), it is possible to construct a wide range of scenarios (Bromm, Coppi & Larson 1999, 2002; Nakamura & Umemura 2001; Abel, Bryan & Norman 2000, 2002; Bromm & Larson 2004; Barkana & Loeb 2000; Wyithe & Loeb 2003; Haiman, Thoul & Loeb 1996; Fryer, Woosley & Heger 2001). Clearly, the first observations of the Dark Ages will have a dramatic impact on our understanding of this new frontier.

In conventional CDM simulations, CSR sources are associated with the cores of massive haloes. Since the distribution of dense peaks collapsing out of an evolving Gaussian density field is well constrained (Miralda-Escudé 2003; Peacock 1999), bright CSR sources are expected to be rare. These will be difficult to find even with well optimized wide-field surveys which exploit large pixels ($\sim 0.1''$). However, the num-

ber of detectable sources above a given flux level at a fixed epoch is more uncertain. This requires a detailed understanding of how and when Ly α emission is produced, and how it manages to escape its immediate environment (Neufeld 1991; Haiman & Spaans 1999). Even the most optimistic calculations (Baron & White 1987) show that Ly α detections will be a major observational challenge on $8 - 10$ m telescopes. The possible discovery of a lensed candidate galaxy at $z = 10$ by Pelló *et al.* (2004) demonstrates the power of lensing to extend our observational reach. However, the total number of sources accessible this way is limited by the small total volume of the universe that is strongly magnified by foreground lenses.

During the Dark Ages, gas accretion onto protogalactic cores must have been well under way. Galactic nuclei at the highest redshifts observed to date ($z \sim 5$) exhibit solar metallicities, and therefore appear to have undergone many cycles of star formation (Hamann & Ferland 1999). Most galaxy cores early in their evolution must have experienced starburst-driven winds. Early protogalactic winds will have carried large amounts of energy, with relatively low dust/metal content, away from the complex circumnuclear environment (Desjacques *et al.* 2004).

In order to understand physical processes associated with the first sources, we will need to resolve the Ly α structures. But, as we now show, detecting emission powered by outflows is a different experimental challenge from that posed by wide-field searches.

¹ On leave from the University of Wollongong

2. THE Ly α CHALLENGE

2.1. Wind-scattered Ly α emission

The difficulty of detecting Ly α during the Dark Ages is emphasized in recent simulations by the GALFORM consortium (Lacey *et al.* 2004; Cole *et al.* 2000). The GALFORM simulations assume that all Ly α is produced by star formation, and that 10% escapes through the action of galactic winds. The simulations are adjusted so as to reproduce the Lyman-break and submillimetre galaxy number counts at presently observed wavelengths. Down to a limiting flux magnitude of $f_{\text{lim}} = 3 \times 10^{-19}$ erg cm $^{-2}$ s $^{-1}$, they predict only about ten sources per square arcmin will be observable across the *entire* redshift range corresponding to the J band. The flux limit is equivalent to a star formation rate of a few solar masses per year which is easily high enough to drive large-scale winds (Heckman 2003; Veilleux 2003).

The most efficient mechanism for Ly α escape is scattering by neutral H entrained in an outflowing wind (Chen & Neufeld 1994). The best observed starburst galaxy M82 reveals UV-scattered bicones along the minor axis (Courvoisier *et al.* 1990; Blecha *et al.* 1990) on a scale of 500 pc to 1 kpc. This corresponds to a spatial scale of 0.1 – 0.2'' at $z \sim 8$. Thus wide-field searches of rare massive haloes will need to exploit pixels on this scale in order to find CSR sources. The scattering wind may be clumped but, as we discuss below, the individual clumps are likely to fall below the detection limit.

2.2. Wind-driven Ly α emission

We now examine the likelihood that most of the Ly α is distributed in small clumps which are cooling out of dissipating gas, and spread over a larger volume than Ly α arising directly from star forming regions.

During the early stages of galaxy formation, collapse is likely to be comparable to star formation as a source of energy for the gas. Cold gas accumulated in the collapse of a small halo (Rees & Ostriker 1977) produces an initial burst of star formation. If the energy released into the nascent interstellar medium by star formation greatly exceeded that released in the collapse, then the bulk of the gas would be unbound from the young galaxy. On the other hand, the mechanical energy required to limit the initial burst of star formation is comparable to the binding energy of the gas, which is roughly the energy needed to significantly rearrange gas within a galaxy. Thus, if the burst of star formation is self-limiting, its feedback cannot fall well short of the binding energy of the gas, *i.e.*, the energy released by the collapse.

Since radiative cooling times of gas at the virial temperature are much shorter than dynamical times in low mass protogalaxies, feedback can only be stored briefly as thermal energy. Energy rapidly lost to radiation is ineffective as feedback. Only feedback energy that is converted to kinetic (and later potential) energy can be effective in limiting star formation on the dynamical timescale. Effective feedback needs to induce rapid large-scale flows, *i.e.*, winds, so we assume that the primary channel of feedback is through winds. This argument requires a moderately high efficiency for the conversion of energy released by star formation into wind energy, but that is consistent with observations of starburst winds (*e.g.*, Strickland & Stevens 2000).

If collapse and the initial burst of star formation make comparable energy inputs to the ISM, we can estimate both using the spherical collapse model. To form a disk, gas must dissi-

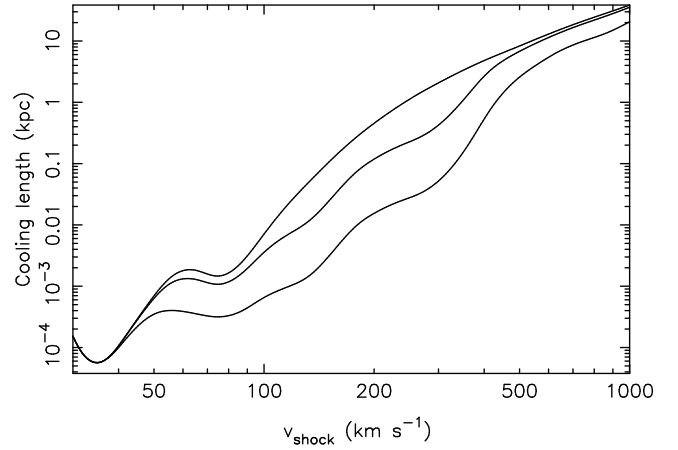


FIG. 1.— Cooling width of a collapse shock at $z = 8$. This shows the product of postshock cooling time and postshock speed as a function of the shock speed, for gas with a pre-shock electron density of 0.036 cm $^{-3}$ and abundances of 0, 0.1 and 1 solar (top to bottom). The cooling width is inversely proportional to pre-shock density.

pate at least the vertical component of its velocity dispersion, *i.e.*, $\sigma^2/2$ per unit mass. For a dissipative collapse — one producing cold gas — the energy dissipated is several times this, so we use the estimate of σ^2 per unit mass dissipated by gas in the collapse. The time taken for a halo to virialize is roughly equal to its turn around time, *i.e.*, half of its collapse time, t_c . If the energy dissipated in the collapse is dissipated in half of the virialization time, the dissipation rate $4M_g\sigma^2/t_c$, where M_g is the gas mass involved in the collapse.

Dark energy is insignificant for collapse at $z \sim 8$, so that the mean density of a halo collapsing at t_c is $3\pi/(Gt_c^2)$, giving the virial radius for a halo of mass M as $R = [GMt_c^2/(4\pi^2)]^{1/3}$. Treating the halo as an isothermal sphere ($GM/R = 2\sigma^2$), then gives $\sigma^2 = 0.5(2\pi GM/t_c)^{2/3}$, so that $\sigma \simeq 53M_{10}^{1/3}$ km s $^{-1}$, where the halo mass $M = 10^{10}M_{10} M_\odot$ and $t_c = 6.27 \times 10^8$ yr [$z = 8$, in Λ CDM with $(h, \Omega_m, \Omega_\Lambda) = (0.7, 0.3, 0.7)$]. Little Ly α can be produced in the collapse unless the gas is heated over $\sim 10^4$ K, *i.e.*, unless $\sigma \gtrsim 10$ km s $^{-1}$, requiring halo masses exceeding $10^8 M_\odot$.

Using the baryon fraction determined by WMAP ($f_b = \Omega_b/\Omega_m \simeq 0.17$; Spergel *et al.* 2003) and assuming that all baryons are gaseous in the collapse, the dissipation rate in the gas during a collapse is $P_d \simeq 4f_b M \sigma^2/t_c \simeq 2 \times 10^{40} M_{10}^{5/3}$ erg s $^{-1}$. Instantaneous dissipation rates will show a significant spread about this value. The fraction emerging as Ly α photons depends on the shock temperature and the fraction of photons that escape. Higher escape fractions are favoured by low optical depth and low abundances (low dust content). In standard Λ CDM, very few $10^{10} M_\odot$ halos collapse before $z = 8$ (Cole *et al.* 2000).

While the fraction of Ly α photons escaping from starbursts is small, a significant part of the energy carried off by galactic winds is ultimately likely to be dissipated in shocks. These are another potential source of Ly α photons and, from above, the energy in the winds is comparable to that dissipated in the collapse. The winds effectively carry energy from the dense, dusty environment of a starburst into lower density regions, where the escape probability for Ly α photons is greater. Starburst wind speeds are high and not strongly dependent on the properties of the hosting halo. This means that if starbursts

are triggered in halos smaller than $10^8 M_\odot$, then the terminating shocks of galactic winds may produce Ly α although the collapse shocks cannot.

From above, the mean baryon density in a dissipationless halo collapsing at $z = 8$ is $3\pi f_b / (Gm_H t_c^2) \simeq 0.036 \text{ cm}^{-3}$, where m_H is the mass of hydrogen. Since dissipation significantly increases the density of the gas, the typical density of gas running into shocks during a dissipative collapse can be somewhat larger than this. The collapse is fairly chaotic and collapsing gas is likely to encounter several shocks before finally reaching its destination. Provided that the effects of radiation transfer are not too significant, the depth of the emitting region behind a radiative shock is approximately equal to the product of the postshock cooling time and velocity. In a strong shock, the gas density is increased by a factor of 4, the speed is decreased by the same factor and the postshock temperature is $T_{ps} = 3\mu m_H v_s^2 / (16k)$, where v_s is the shock speed and μm_H is the mean mass per particle. Fig. 1 shows the width of the postshock cooling region for a preshock electron density of 0.036 cm^{-3} , for metal abundances of 0, 0.1 and 1 solar.

Initially, the collapsing gas flow may be coherent on larger scales than the postshock cooling length in Fig. 1. In that case, cooling shocked regions are sheetlike and emission is brightest at caustics where we see folds in these sheets projected onto the sky. The cooling gas is subject to thermal and other instabilities that will generally cause it to fragment on about the scale of the cooling length. (The flow into any further shocks is likely to be considerably more chaotic.) For haloes in the mass range of interest, the shock speeds in the collapse are, at most, $100 - 200 \text{ km s}^{-1}$. In a pristine gas, the inferred size of cooling clumps is roughly 100 pc, or $0.02''$ at a redshift of $z \sim 8$. The small size of the cooling region demands an infrared imager which utilizes small pixels ($\sim 0.01''$) and adaptive optics correction. However, we point out that rapid winds from starbursts can produce significantly larger cooling regions.

Since gas is compressed significantly in a dissipative collapse, the time scale for star formation in a clump of collapsed gas can be much shorter than the dynamical time of the collapsing system ($\sim 10^8 \text{ yr}$). Massive stars take only $\sim 10^6 \text{ yr}$ to produce supernovae, giving plenty of time for starbursts and their winds to get underway while other gas continues to collapse into the system. Interaction between infalling gas and starburst winds can lead to further shocking of both. This process is observed in M82 where the outflowing starburst-driven wind impinges directly on infalling gas at a radius of 11 kpc (Yun, Ho & Lo 1994) producing observable H α and x-ray emission (Devine & Bally 1999; Lehnert, Heckman & Weaver 1999).

3. EXPECTED Ly α SURFACE BRIGHTNESS

We now examine whether wind-powered Ly α emission in small clumps can be detected with an 8m telescope using an adaptive optics imager with small pixels ($0.02''$). We assume that the total energy released in Ly α at a fixed star formation rate is comparable to what is generated in large-scale shocks driven by the starburst, and that this emission escapes without attenuation. As discussed in §2.2, this assumes a high conversion rate of the supernova energy into wind energy (e.g., Strickland & Stevens 2000).

From surveys of nearby dwarf galaxies (Martin 2003; Velleux 2003), we adopt a wind radius of 5 kpc. At $z \sim 8$, the shock occurs at $1''$ radius and is barely resolved. Naively, if the wind energy escapes along bipo-

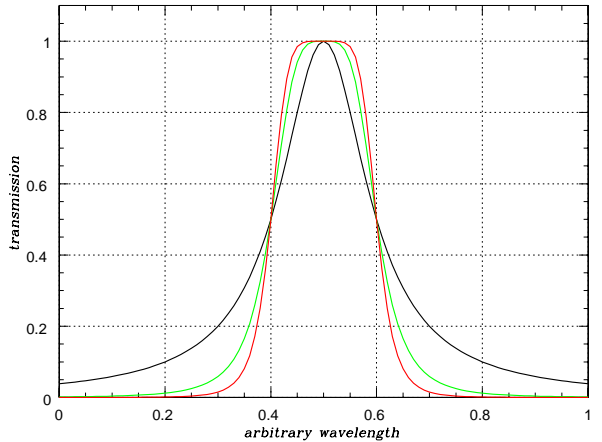


FIG. 2.— Filter profiles used in our GSAOI calculations. The Lorentzian profile ($m = 1$) shown in black is the expected response of a high finesse ($N=40$) tunable filter. The green profile ($m = 2$) is the low-cost filter option, the blue profile ($m = 3$) is the high-cost filter option.

lar cones, the Ly α surface brightness will be increased by the decrease in solid angle compared to a spherical wind. This factor can be ~ 10 since most winds appear to be highly collimated (Shoppell & Bland-Hawthorn 1998; Sugai, Davies & Ward 2003). However, this factor does not apply to a comparison with the expected flux from a CSR, since the normal assumption is that the collimated wind material is what renders the central source visible. An escape fraction of 10% assumed in the GALFORM simulations is the fraction of radiation which escapes along the bicones multiplied by the fraction scattered in the wind.

For wind-induced emission, in our model, the total power available is $10 f_{\text{lim}}$ but this is now spread over many more pixels. The surface brightness of the shock induced Ly α emission depends critically on how the bipolar shock surfaces are oriented with respect to the observer. If the bipolar wind lies in the plane of the sky, most of the emission is confined to limb-brightened arcs over an area of $\sim 10^2$ pixels depending on the curvature of the shock surface. If the bipolar wind is directed at the observer, the projected radius of the shocked-induced nebula is half the intrinsic radius (60° opening angle). Thus, the flux is now dispersed over an area of $\sim 10^3$ pixels.

Our expectation is that the Ly α flux *per pixel* will be an order of magnitude fainter in external large-scale shocks (ELS) compared to CSR emission in a large pixel survey ($0.1''$). We believe that it will be important to reach this flux level if we are to understand the nature and origin of the Ly α emission. We have assumed that essentially all of the Ly α emission escapes its environs since it is produced *in situ*. But in the presence of any diffuse intergalactic HI component at rest with the expanding universe, the shock surface must have a sufficient redshift in order for the Ly α emission to escape to the observer.

We have already noted that CSR emission is rendered visible through scattering by neutral H in the wind. From the lo-

TABLE 1
BASIC COSMOLOGICAL PARAMETERS FOR THE FOUR DARK J-BAND
WINDOWS.

| | | | | |
|--|-------|-------|-------|-------|
| Wavelength (μm) | 1.06 | 1.12 | 1.19 | 1.26 |
| Redshift | 7.72 | 8.22 | 8.79 | 9.37 |
| Time since Big Bang (Gyr) | 0.66 | 0.60 | 0.55 | 0.51 |
| Time before present (Gyr) | 12.80 | 12.85 | 12.91 | 12.95 |
| Physical scale (kpc/arcsec) | 4.92 | 4.73 | 4.53 | 4.35 |
| Luminosity distance, d_L (Mpc) | 77283 | 82979 | 89667 | 96398 |
| Flux, $F = L_S/4\pi d_L^2$ (10^{-19} cgs) ^a | 1.40 | 1.21 | 1.04 | 0.90 |
| Physical depth, D (Mpc/1000 km s ⁻¹) | 1.009 | 0.929 | 0.849 | 0.779 |
| Comoving depth, D_o (Mpc/1000 km s ⁻¹) | 8.798 | 8.565 | 8.312 | 8.078 |
| Physical volume, $1' \times 1' \times D$ (Mpc ³) | 0.088 | 0.075 | 0.063 | 0.053 |
| Comoving volume, $1' \times 1' \times D_o$ (Mpc ³) | 58.5 | 58.7 | 59.0 | 59.1 |

NOTE. — The cosmology is $(h, \Omega_m, \Omega_\Lambda) = (0.7, 0.3, 0.7)$. The comoving volume is essentially constant over the windows and the total timespan is only 150 Myr.

^aThe expected flux from a source with luminosity $L_S = 10^{41}$ erg s⁻¹, in units of 10^{-19} erg cm⁻² s⁻¹, only varies by 50%.

cal universe, we know that winds arise from highly inhomogeneous starburst cores and entrain most of their mass from cooler material in the surrounding disk (Suchkov *et al.* 1996). Thus the scattering medium is likely to be highly clumped. However, since the total escaping Ly α flux in our model is f_{lim} , these scattering clumps are likely to be an order of magnitude fainter than self-illuminating clumps of shocked gas induced by the same wind.

4. SURVEY METHOD

4.1. Wide-field Ly α survey

We envisage an initial survey with a wide-field, large-pixel imager which scans over several fields in order to identify an initial list of CSR sources. This is the primary motivation of the DAZLE instrument under construction at the Institute of Astronomy, University of Cambridge for the Very Large Telescope (Bland-Hawthorn *et al.* 2003, see also <http://www.ast.cam.ac.uk/~optics/dazle>) which exploits high performance $\mathcal{R} = 1000$ interference filters closely spaced in wavelength within the J band. The wide-field (6.9' square) observations are built up in interleaved sub-exposures by switching between the two filters: the images are then differenced in order to detect signals in one band that are not evident in the other. This technique has been widely used with the Taurus Tunable Filter (TTF) on the AAT and has led to the identification of a line-emitting populations out to $z \sim 5$ (*e.g.*, Barr *et al.* 2004).

Each target field with DAZLE will require long exposures, and may require several fields in order to find a single source. Table 1 summarises the cosmological properties of the four 'dark' windows in the J-band originally identified in the DAZLE design study (Cianci 2003, see also <http://www.aao.gov.au/dazle>) which are clearly evident in Fig. 3.

We now present SNR calculations for a wide-field and an adaptive optics near-IR imager on an 8m telescope. The calculations utilize both airglow and absorption spectra at a spectral resolution of $\mathcal{R} = 10\,000$ (*cf.* Offer & Bland-Hawthorn 1998). We adopt instrumental parameters for DAZLE and for the Gemini South Adaptive Optics Imager (GSAOI) to be commissioned in 2005: the key numbers are listed in Table 2 (McGregor *et al.* 2003). Note that several of the parameters are expressed over a range: the lower value is used

TABLE 2
BASIC PARAMETERS FOR GSAOI AND A DAZLE-LIKE INSTRUMENT
OPERATING AT THE GEMINI TELESCOPE.

| | |
|------------------------|---|
| Reduced telescope area | $(\pi/4)(7902 - 1302)^2$ cm ⁻² |
| System throughput | 0.27 |
| Filter throughput | 0.80 |
| Detector pixel size | 0.02" – 0.1" |
| Detector read noise | 5 e ⁻ pix ⁻¹ |
| Detector dark current | 0.003 – 0.05 e ⁻ s ⁻¹ pix ⁻¹ |
| Night-glow continuum | 2 – 5 Rayleigh Å ⁻¹ |
| Source flux | 3 – 30 $\times 10^{-20}$ erg cm ⁻² s ⁻¹ |
| Source diameter | 0.04" – 0.20" |
| Total SNR for source | 3 – 5 |
| Exposure time | 3600 s |

NOTE. — For parameters shown over a range, the lower bound is specific to the ELS (GSAOI) case, the upper bound refers to the CSR (DAZLE) case. The one exception is the night sky continuum where we incorporate both bounds in both calculations. The reduced telescope area incorporates the loss due to the Cassegrain hole (M2 stop). The filter throughput assumes an IR detector that cuts off at 2.5 μm ; this reduces to 60% for a detector cut-off at 5 μm due to the need for additional optical density layers for long wavelength suppression. The exposure time determines the number of read noise contributions to the summed image.

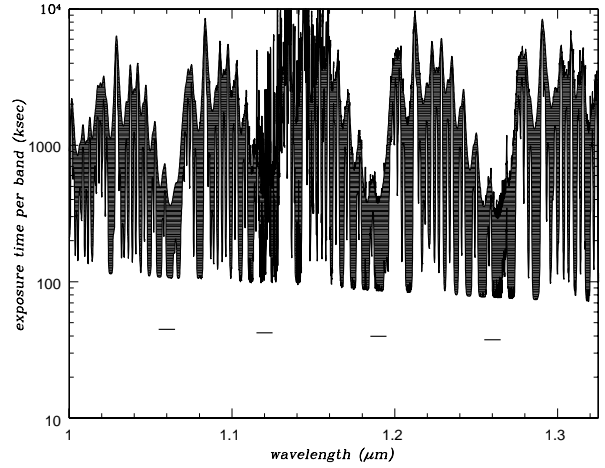


FIG. 3.— The calculated total exposure times (in ksec) for the parameters listed in Table 2. The solid horizontal lines are the times to reach SNR = 5 in an initial DAZLE survey. The filled region shows the expected times to reach SNR = 3 in a targeted study with GSAOI: the lower envelope is for a filter with $m = 3$, $\mathcal{R} = 1000$; the upper envelope is for $m = 1$, $\mathcal{R} = 500$. The dark windows near 1.06 μm , 1.19 μm and 1.26 μm are the most suitable for Ly α observations; note how the upper envelope picks these out. The cosmological parameters for these four windows are given in Table 1.

in our ELS calculation (GSAOI), and the upper value is used in our CSR calculation (DAZLE). The GSAOI will utilise a HAWAII-2RG array, under development for the James Webb Space Telescope, which is expected to have exceptionally low dark current. DAZLE exploits a HAWAII-2 array which has a much higher dark current, but which is adequate for wide-field surveys, as we show below.

The equivalent luminosity for the quoted Ly α flux and the physical size of the Ly α blobs is given in Table 1 as a function of redshift. Since the blob sizes in our calculations are larger than the AO-corrected psf of GSAOI, we do not consider the J-band Strehl ratio in our calculations. The J-band airglow spectrum was normalized to the expected J-band counts given in McGregor *et al.* (2003). We consider two limiting cases

for the night-glow continuum between the OH lines (*e.g.*, Content 1996); the actual night-glow continuum level is unknown but is bracketed by the quoted values in Table 2. The night-glow surface brightness is quoted in Rayleighs (R) per Angstrom where $1 \text{ R} = 10^6/4\pi \text{ phot cm}^{-2} \text{ s}^{-1} \text{ sr}^{-1}$.

At a fixed spectral bandpass defined by \mathcal{R} , the wings of the filter profile must be considered. Jones, Bland-Hawthorn & Burton (1996) demonstrate that the out-of-band blocking of an interference filter with m cavities is closely matched to a Butterworth function of degree m . We have incorporated the Butterworth profile (see Fig. 2) in our calculations. The single cavity ($m = 1$) is the Lorentzian profile of a tunable filter in the high finesse limit (Bland-Hawthorn & Jones 1998). The relatively low-cost DAZLE filters utilise $m = 2$ (two cavity), although there is also a high-cost option with $m = 3$. We assume that placement within the instrument does not degrade the effective bandpass, an issue discussed at length by Bland-Hawthorn *et al.* (2001).

Both $m = 2$ and $m = 3$ filters are risky and highly expensive items to manufacture since the multi-cavity dielectric coatings can exceed $10\mu\text{m}$ in total thickness, requiring hundreds or even thousands of layers. As was found in the DAZLE study, this can be greatly exacerbated by the need for high optical density to achieve long-pass blocking² by the interference filter.

In Fig. 3, the horizontal lines indicate we need 40 ksec per field in order to achieve a 5σ detection in one or other band, but note that the DAZLE technique surveys twice the volume of a single $\mathcal{R} = 1000$ filter image. (If the detection relies on the differencing of on-line and off-line bands, its statistical significance is reduced to 3.5σ .) An (almost) equivalent strategy is to halve the exposures per field, and to observe two fields in two closely spaced bands. Once tentative sources have been identified, in order for the emission to be $\text{Ly}\alpha$, the source should not be evident in deep *ugriz* images (*i.e.*, $\text{AB mag} \gtrsim 28$) corresponding to rest-frame Lyman continuum.

4.2. Targetted $\text{Ly}\alpha$ survey

The initial wide-field survey will do little more than identify tentative sources for closer study. At this point, we target specific sources for further study with a high resolution imager and adaptive optics. The initial survey will need to target fields in the vicinity of IR-bright stars which can be utilised for AO correction. A particular advantage of narrowband filters is that the AO correction is not hampered by atmospheric refraction which can spread point sources over tens of pixels within a broadband filter.

For a targetted study, we require only a single narrowband filter, and need only achieve 3σ per blob within the $\text{Ly}\alpha$ nebula to map the distribution of ionized gas. But Fig. 3 shows that the total exposure times per source are 100 ksec. At $\mathcal{R} = 1000$, there appear to be a dozen useful windows within the J-band. However, in our design study for DAZLE (Cianci 2003), we find that only 3–4 windows are practical. For a filter placed at the pupil, there is a slight phase effect over the field such that the passband at the filter edge is bluer than at the centre of the field. For a filter placed in the converging beam, the passband is broadened slightly.

Another concern is the difficulty of manufacturing a 0.1λ narrowband filter centred at the prescribed wavelength. Given

² An alternative strategy is to exploit an IR array with a sensitivity cut-off at a shorter wavelength ($\lambda < 2\mu\text{m}$). If the dark current can be kept to a minimum, we see this approach as preferable to a HAWAII-2RG array.

the restricted tuning capability of an interference filter, and its degraded performance on tilting, it is tempting to consider a tunable filter for $\text{Ly}\alpha$ imaging. However, the upper envelope of the filled region in Fig. 3 shows the expected poor performance of a filter profile with Lorentzian wings.

The above considerations require that we accept a window which is actually twice as broad as the design bandwidth. In Fig. 3, we note that there is only a handful of good windows available at $\mathcal{R} = 500$. In terms of photometric stability, the windows near $1.06\mu\text{m}$, $1.19\mu\text{m}$ and $1.26\mu\text{m}$ are the most ideal. The window at $1.12\mu\text{m}$ suffers from variable and complex atmospheric absorption. The relevant cosmological parameters for these four windows are given in Table 1.

The $1.12\mu\text{m}$ window could be recovered if two IR arrays were placed side by side in the image plane, and these devices were moved back and forth every few mins, in synchrony with nodding by the telescope, such that we build up two separate fields of view. This mechanical form of ‘nod & shuffle’ (*cf.* Glazebrook & Bland-Hawthorn 2001) would average out atmospheric effects, and at the same time minimize the read noise penalty, although it incurs a $\sqrt{2}$ penalty from dark current noise.

If systematics can be controlled, the long total exposure times of 30 hr per field are not unreasonable. If there are weak OH features in the dark windows, these are likely to be variable and may define the systematic noise limit. Note that if pixel stability dominates the noise limit, a Dark Age experiment cannot be carried out since this leads to short exposures (Fowler-8 sampling) and results in a huge read noise penalty. However, D. B. Hall (2003, personal communication) has found that the HAWAII-2RG arrays have comparable stability to some of the best optical detectors.

5. THE IMPORTANCE OF DARK CURRENT

We now show that the IR arrays specified in Table 2 are ideally suited to the proposed experiments. If the J-band windows are truly dark, the read + dark noise contribution defines the limiting sensitivity we can reach. This is illustrated in Fig. 4 which shows the total exposure time required in the $1.06\mu\text{m}$ window to achieve $\text{SNR} = 3$ on a $\text{Ly}\alpha$ blob with a total flux of $3 \times 10^{-20} \text{ erg cm}^{-2} \text{ s}^{-1}$. Here we assume a filter with $\mathcal{R} = 1000$ and $m = 3$. This calculation is specific to GSAOI: the pixels are $0.02''$ and the read noise is 5 e^- . At the top of the figure, the blobs are spread over many pixels which greatly increases the effective background from dark current.

The results are only weakly sensitive to the number of separate exposures since the dark current noise dominates for exposures longer than about 500 sec. Note in particular how a targetted study with GSAOI benefits from a very low dark current array (d.c. $< 0.01 \text{ e}^- \text{ s}^{-1} \text{ pix}^{-1}$) for essentially any blob size. The HAWAII-2RG array has demonstrably the lowest dark current of any existing or planned array technology (D.B. Hall 2003, personal communication).

In Fig. 5, we show the total exposure time required in the $1.06\mu\text{m}$ window to achieve $\text{SNR} = 5$ on a $\text{Ly}\alpha$ blob with a total flux of $3 \times 10^{-19} \text{ erg cm}^{-2} \text{ s}^{-1}$. This calculation is specific to the initial DAZLE survey with $\mathcal{R} = 1000$ and $m = 3$. Note how the uncertainty in the dark sky continuum leads to some uncertainty in the detectability of $\text{Ly}\alpha$ blobs. For CSR source sizes of $0.2''$, the existing HAWAII-2 arrays are well suited to wide-field $\text{Ly}\alpha$ surveys of this kind.

The implication here is that the pixel size must be well matched to the expected size of the $\text{Ly}\alpha$ emitting regions. If the pixels are much larger than the emitting blobs, night-glow

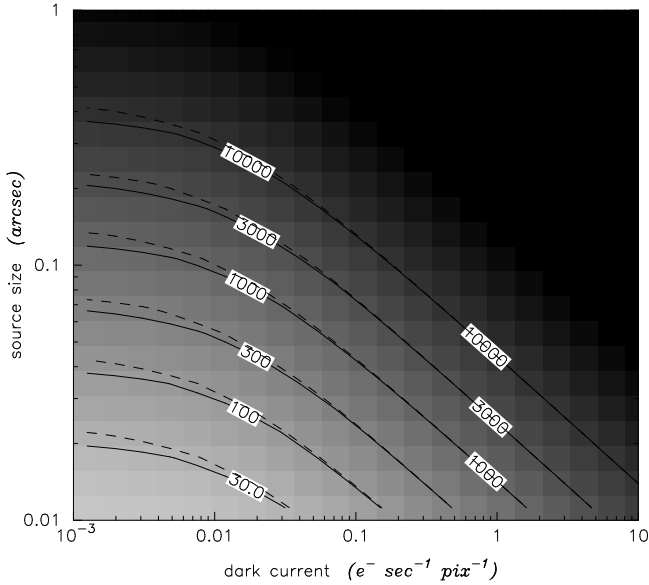


FIG. 4.— Total exposure times (in ksec) in the $1.06\mu\text{m}$ window as a function of dark current (horizontal) and blob size (vertical; in arcsec) for a detector with $0.02''$ pixels. We use the parameters in Table 2 specific to GSAOI. The exposure times assume $\text{SNR}=3$ per source for a total object flux of $3 \times 10^{-20} \text{ erg cm}^{-2} \text{ s}^{-1}$. Note the importance of very low dark current in order to detect clumpy $\text{Ly}\alpha$ emission. The solid lines assume a high level of night-glow continuum between the OH lines (see Table 2), the dashed lines assume weak night-glow.

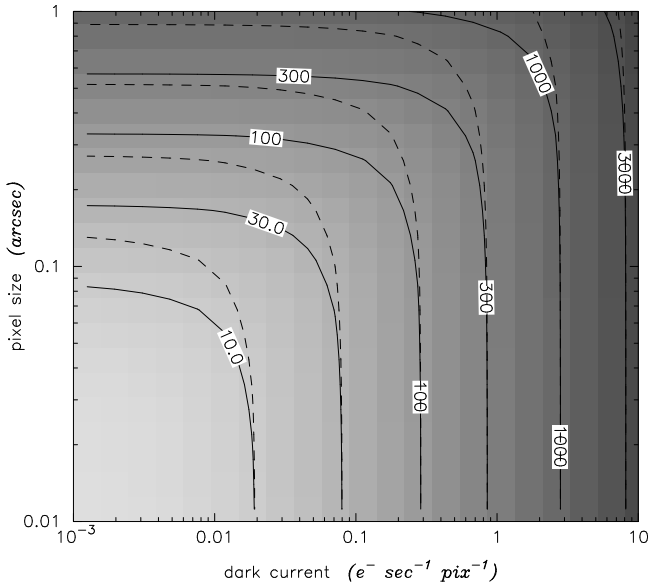


FIG. 5.— Total exposure times (in ksec) in the $1.06\mu\text{m}$ window as a function of dark current (horizontal) and pixel size (vertical; in arcsec). We use the parameters in Table 2 specific to a DAZLE-like instrument. The exposure times assume $\text{SNR}=5$ per source for a total object flux of $3 \times 10^{-19} \text{ erg cm}^{-2} \text{ s}^{-1}$. The solid lines assume a high level of night-glow continuum between the OH lines (see Table 2), the dashed lines assume weak night-glow. For $0.2''$ source diameters, existing HAWAII-2 arrays are well suited to wide-field searches.

continuum will dominate the exposure and result in excessively long exposures. If the emitting blobs are much larger than the pixels, dark current dominates leading to excessively long exposures.

6. CONCLUDING REMARKS

It is clear that something quite extraordinary took place over a time span of a few hundred million years which led to the complete ionization of the intergalactic medium. The epoch of (re)ionization is likely to attract a great deal of attention over the coming decade.

We have shown that detecting sources beyond $z = 7$ is going to be very challenging on 8 – 10m telescopes. But since 30 – 100m telescopes will not be in operation until the next decade, narrowband imaging is likely to dominate studies of the Dark Ages for years to come. We have outlined a strategy based on wide-field surveys to identify star formation in massive haloes, followed by detailed studies with an adaptive optics imager. The optimal technologies for both kinds of study will be available in the next few years.

It is often observed that major discoveries are made within five years of a new technology (*e.g.*, Harwit 1981). What is less well known is that this statement normally applies to experiments which achieve the systematic noise limit of the apparatus. Glazebrook & Bland-Hawthorn (2001) argue that the systematic limit possible with nod & shuffle spectroscopic observations argues for total integration times measured in months or even years. Since large telescopes are general user facilities, it is relatively rare that hundreds of hours are devoted to a single target field. But in order to reach back to the Dark Ages, observing programmes of one or two weeks at a time will be essential.

PEJN was partly supported by NASA grant NAS8-01130. JBH would like to thank Warrick Couch and Doug Simons for the impetus to think about Dark Age science in the context of Gemini, and to the GSAOI team at Mount Stromlo (PI: Peter McGregor) for their excellent work.

REFERENCES

- Abel, T., Bryan, G. L., & Norman, M. L. 2000, *ApJ*, 540, 39
- Abel, T., Bryan, G. L., & Norman, M. L. 2002, *Science*, 295, 93
- Barkana, R., & Loeb, A. 2000, *ApJ*, 539, 20
- Baron, E., & White, S. D. M. 1987, *ApJ*, 322, 585
- Barr, J. M., *et al.* 2004, submitted to *MNRAS*
- Bland-Hawthorn, J. & Jones, D. H. 1998, *PASA*, 15, 44
- Bland-Hawthorn, J., van Breugel, W., Gillingham, P. R., Baldry, I. K., & Jones, D. H. 2001, *ApJ*, 563, 611
- Bland-Hawthorn, J. 2003, *AAO Newsletter*, 103, 16

- Blecha, A., Golay, M., Huguenin, D., Reichen, D., & Bersier, D. 1990, A&A, 233, L9
- Bromm, V., Coppi, P. S., & Larson, R. B. 1999, ApJ, 527, L5
- Bromm, V., Coppi, P. S., & Larson, R. B. 2002, ApJ, 564, 23
- Bromm, V. & Larson, R. B. 2004, ARAA, in press
- Chen, W. & Neufeld, D. A. 1994, ApJ, 432, 567
- Cianci, S. 2003, PhD, University of Sydney
- Cole, S., Lacey, C. G., Baugh, C. M., & Frenk, C. S. 2000, MNRAS, 319, 168
- Content, R. 1996, ApJ, 464, 412
- Courvoisier, T. J.-L., Reichen, M., Blecha, A., Golay, M., & Huguenin, D. 1990, A&A, 238, 63
- Desjacques, V., Nusser, A., Haehnelt, M. G., & Stoehr, F. 2004, MNRAS, astro-ph/0311209
- Devine, D., & Bally, J. 1999, ApJ, 510, 197
- Fan, X. *et al.* 2000, AJ, 120, 1167
- Fan, X. *et al.* 2003, AJ, 125, 1649
- Fryer, C., Woosley, S. E., & Heger, A. 2001, ApJ, 550, 372
- Glazebrook, K., & Bland-Hawthorn, J. 2001, PASP, 113, 197
- Gnedin, N. Y. & Ostriker, J. P. 1997, 486, 581
- Haiman, Z. & Loeb, A. 1998, ApJ, 503, 505
- Haiman, Z. & Spaans, M. 1999, ApJ, 518, 138
- Haiman, Z., Thoul, A. A. & Loeb, A. 1996, ApJ, 464, 523
- Hamann, F. & Ferland, G. 1999, ARAA, 37, 487
- Harwit, M. 1981, Cosmic Discovery, New York: Basic Books
- Heckman, T.M. 2003, In Galaxy Evolution: Theory & Observations, eds V. Avila-Reese, C. Firmani, & C. Allen, Rev. Mex. A. A., 17, 47
- Jones, D. H., Bland-Hawthorn, J., & Burton, M. G. 1996, PASP, 108, 929
- Kneib, J.-P., Ellis, R. S., Santos, M. R., & Richard, J. 2004, ApJ, astro-ph/0402319
- Kogut, A. *et al.* 2003, ApJS, 148, 161
- Lacey, C. *et al.* 2004, in preparation
- Lehnert, M., Heckman, T. M., & Weaver, K. A. 1999, ApJ, 523, 575
- Loeb, A., & Barkana, R. 2001, ARAA, 39, 19
- McGregor, P. *et al.* 2003, GSAOI Critical Design Review Vol. 2 (84699-GEM00334)
- Martin, C.L. 2003, In Galaxy Evolution: Theory & Observations, eds V. Avila-Reese, C. Firmani, & C. Allen, Rev. Mex. A. A., 17, 56
- Miralda-Escudé 2003, Science, 300, 1904
- Nakamura, F., & Umemura, M. 2001, ApJ, 548, 19
- Neufeld, D. A. 1991, ApJ, 370, L85
- Offer, A. R. & Bland-Hawthorn, J. 1998, MNRAS, 299, 176
- Peacock, J.A. 1999, Cosmological Physics, CUP
- Pelló, R., Schaerer, D., Richard, J., Le Borgne, J.-F., & Kneib, J.-P. 2004, A&A, 416, L35 (astro-ph/0403025)
- Rees, M. J., & Ostriker, J. P. 1977, MNRAS, 179, 541
- Shopbell, P. L., & Bland-Hawthorn, J. 1998, ApJ, 493, 129
- Spergel, D. N. *et al.* 2003, ApJS, 148, 175
- Strickland, D., & Stevens, M. R. 2000, MNRAS, 314, 511
- Suchkov, A. A., Berman, V. G., Heckman, T. M., & Balsara, D. S. 1996, ApJ, 463, 528
- Sugai H., Davies, R. I., & Ward, M. J. 2003, ApJ, 584, L9
- Veilleux, S. 2003, In Recycling Intergalactic and Interstellar Matter, IAU Symp. 217, 168
- Wyithe, S., & Loeb, A. 2003, ApJ, 588, L69
- Wyithe, S., & Loeb, A. 2004, Nat, in press
- Yun, M. S., Ho, P. T. P., & Lo, K. Y. 1994, Nat, 372, 530